

THE DISTRIBUTION OF MARS WATER VAPOR VERSUS ALTITUDE, SEASON, AND LATITUDE AS DERIVED FROM GLOBAL COMPARISONS OF CRISM RETRIEVED AND LMDGCM SIMULATED $O_2(^1\Delta_g)$ DAYGLOW PROFILES

R. T. Clancy, B. Sandor, M. Wolff, *SSI, Boulder CO (clancy@spacescience.org)*, F. Lefèvre, T. Navarro, *LATMOS, Paris*, M. Smith, *GSFC, Greenbelt, MD*, T. McConnochie, *UofMD, College Park, MD*, S. Murchie, H. Nair, and A. Toigo, *JHU/APL, Columbia, MD*.

Introduction:

A unique, global set of CRISM VIS/near-IR (0.4-4 μm) limb spectral scans has accumulated over the continuing 2009-2016 (MY29-33) period. Polar nightglow profiles for $O_2(^1\Delta_g)$ band (1.27 μm) and OH Meinel band emission among these full orbit (full latitudinal) limb coverages provide indications of some accuracy in the LMD (Laboratoire de Météorologie Dynamique) GCM (General Climate Model) simulation of mesospheric (50-100 km) meridional transport of atomic H and O (Clancy et al., 2012, 2014). Distinct $O_2(^1\Delta_g)$ dayglow appears over sunlit latitudes that is strongly, inversely related to atmospheric water vapor (Barth et al, 1973; Parkinson and Hunten, 1973; McElroy and Donahue, 1972; Guslyakova et al., 2016).

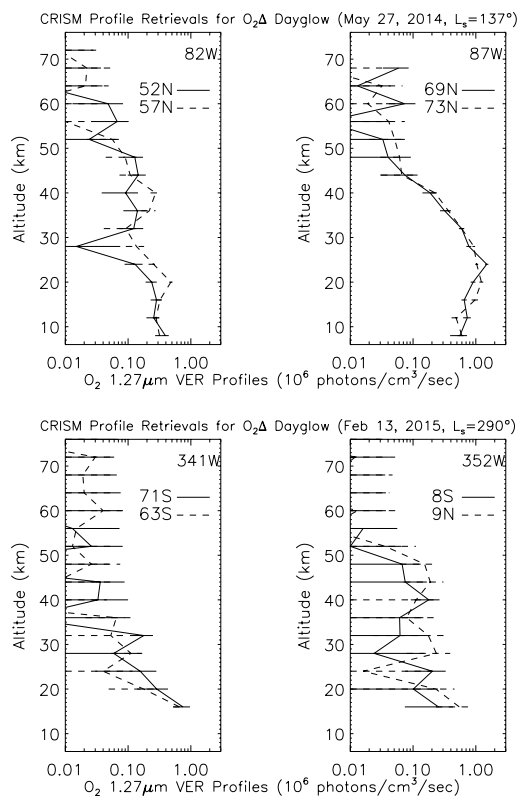


Figure 1. Vertical profiles of CRISM retrieved $O_2(^1\Delta_g)$ VER for $L_s=137^\circ$ (top) and 290° (bottom).

Dedicated limb-scattering radiative transfer profile retrievals for $O_2(^1\Delta_g)$ volume emission rates (VER) have been applied to > 1000 CRISM near-IR spectral limb scans extending over the full range of sunlit latitudes, for 2-5

surface longitude corridors, for fairly complete seasonal (L_s) coverage as accumulated over MY29-33, and over 8-80 km altitudes (Clancy et al., 2016). Two key results follow from point-by-point comparisons of CRISM retrieved versus LMDGCM simulated $O_2(^1\Delta_g)$ VER for the full set of CRISM limb profile retrievals.

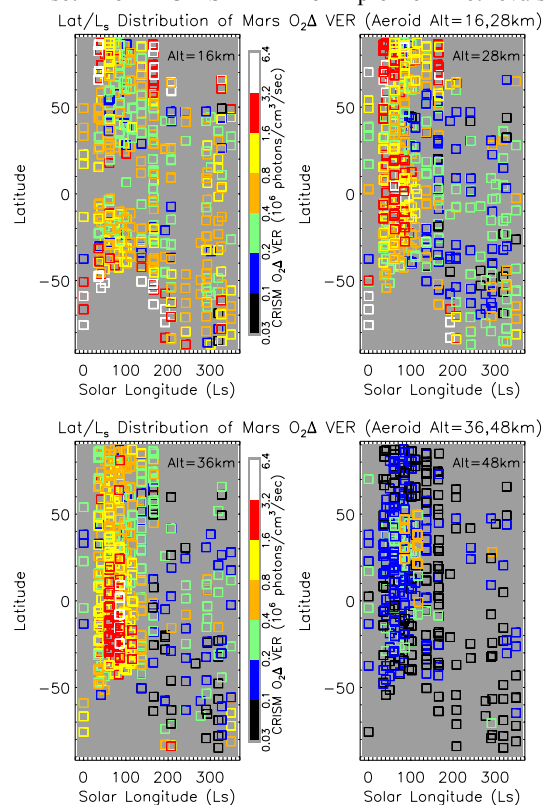


Figure 2. The latitude/ L_s distributions of CRISM retrieved $O_2(^1\Delta_g)$ VER for aeroid altitude levels of 16, 28 km (top) and 36, 48 km (bottom).

Model-data comparisons for altitude at or below 20 km attitude indicate a much smaller rate coefficient for collisional de-excitation of $O_2(^1\Delta_g)$ by CO_2 collisions ($0.25 \pm 0.25 \times 10^{-20} \text{ cm}^3 \text{ sec}^{-1}$) than reported by Guslyakova et al (2016; $0.73 \times 10^{-20} \text{ cm}^3 \text{ sec}^{-1}$).

The second result regards the current presentation, the inference of the vertical/latitudinal distribution of the Mars water vapor versus season over ~10-60 km altitudes, based on scaling the LMDGCM simulated water vapor distribution by the ratio of CRISM retrieved to LMDGCM simulated $O_2(^1\Delta_g)$ VER. The distinctive character of inferred changes to simulated water vapor distributions indicates a range of transport and saturation shifts over specific seasons and processes.

CRISM $O_2(^1\Delta_g)$ Dayglow Profiles:

Figures 1 and 2 present a range of CRISM retrieved $O_2(^1\Delta_g)$ VER profiles over sunlit latitudes and seasons, in terms of individual profiles (figure 1) and the full set of CRISM $O_2(^1\Delta_g)$ VER interpolated to aroid altitude levels of 16, 28, 36, and 48 km (figure 2). Strong vertical, orbital (solar longitude, L_s) and latitudinal variations in $O_2(^1\Delta_g)$ VER are associated with water vapor variations in the Mars atmosphere. $O_2(^1\Delta_g)$ dayglow reflects ozone (O_3) photolysis, which is inversely proportional to water vapor photolysis products.

Figure 3 presents latitude/altitude distributions for the ratio of CRISM retrieved to LMDGCM modeled $O_2(^1\Delta_g)$ VER for seasonal/orbital binned periods of $L_s=30-60^\circ$ and $60-140^\circ$ (top), and $200-310^\circ$ and $320-360^\circ$ (bottom).

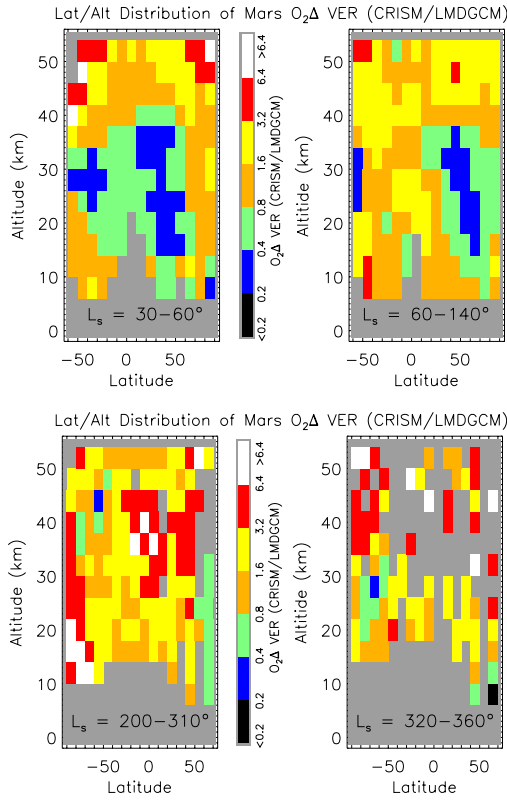


Figure 3. Latitude/altitude distributions for the ratio of retrieved (CRISM) to simulated (LMDGCM) ($O_2(^1\Delta_g)$) VER for Mars seasonal ranges: northern spring (top left), northern summer (top right), southern summer (bottom left) and southern spring (bottom right).

Several altitude/latitude/ L_s patterns are indicated in figure 3. 1) CRISM $O_2(^1\Delta_g)$ VER are 2-3 times larger than model values above 35-40 km for all seasons, 2) At 15-35 km altitudes, LMDGCM $O_2(^1\Delta_g)$ VER are 2-3 times larger than CRISM values for most latitudes in northern spring, and for northern mid-to-high latitudes in northern summer, and 3) CRISM $O_2(^1\Delta_g)$ VER are 2-6 times larger than model values over southern summer mid-to-high latitudes for altitudes of 10-30 km. These differences in observed/modeled $O_2(^1\Delta_g)$ VER are closely related to differences in observational (i.e., actual) and modeled water vapor, which supports inference of water vapor as a function of altitude, latitude, and L_s .

Inferred Mars Water Distributions:

Figure 4 presents the LMDGCM $O_2(^1\Delta_g)/H_2O$ correlation for locations (latitude, longitude, altitude) and times (LT near 3pm, L_s) corresponding to CRISM measurements. The two quantities are inversely proportional over 2 orders-of-magnitude variation, and narrowly so for fixed temporal/location bins (right panel). This fairly robust anti-correlation between $O_2(^1\Delta_g)$ VER and H_2O abundance supports a correspondingly robust derivation of the global (latitude/altitude/ L_s) distribution of Mars atmospheric water vapor over ~ 10 to 60 km altitudes.

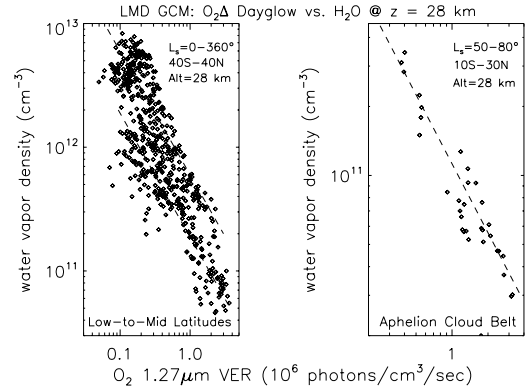


Figure 4. LMDGCM photochemical simulations (Lefèvre et al., 2004, 2008) of $O_2(^1\Delta_g)$ VER versus water vapor, for the locations/times of all low-to-mid latitude (left) and aphelion cloud belt (right) CRISM retrievals at 28 km aroid altitude.

Figures 5-8 present the LMDGCM simulated (left panels) versus CRISM $O_2(^1\Delta_g)$ -scaled (right panels) latitudinal/altitude distribution for Mars water vapor as averaged over seasonal periods of $L_s = 30-60^\circ$, $60-140^\circ$, and $200-310^\circ$, respectively. Distinct changes to the modeled water vapor distribution, as a function of season (L_s), latitude, and altitude, correspond to the ratio of observed/modeled $O_2(^1\Delta_g)$ VER presented in figure 3. These water vapor

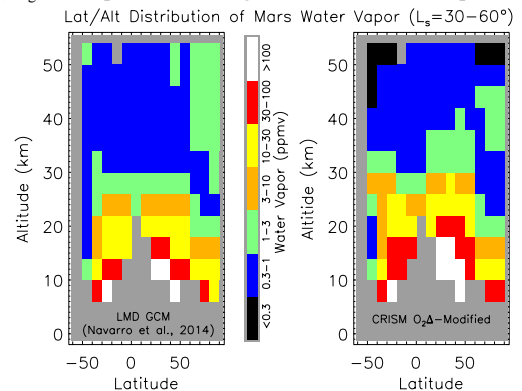


Figure 5. LMDGCM simulated (Navarro et al., 2014) and CRISM $O_2(^1\Delta_g)$ -scaled water vapor latitude/longitude distributions, averaged over northern spring ($L_s=30-60^\circ$).

changes can in turn be qualitatively associated with changes to model processes, such as transport and microphysics.

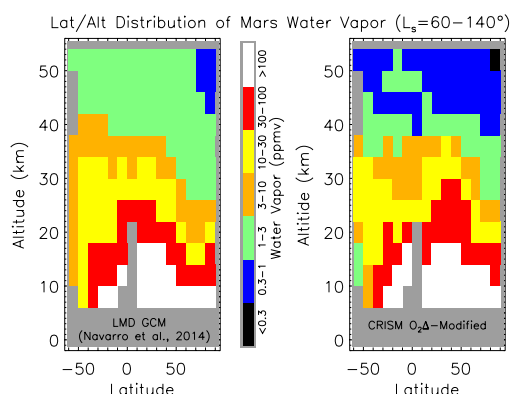


Figure 6. LMDGCM simulated (Navarro et al., 2014) and CRISM $O_2(\Delta_g)$ -scaled water vapor latitude/longitude distributions, averaged over northern summer ($L_s=60-140^\circ$).

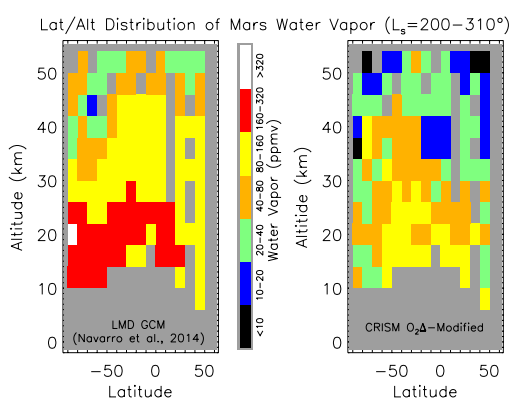


Figure 7. LMDGCM simulated (Navarro et al., 2014) and CRISM $O_2(\Delta_g)$ -scaled water vapor latitude/longitude distributions, averaged over southern summer ($L_s=200-310^\circ$).

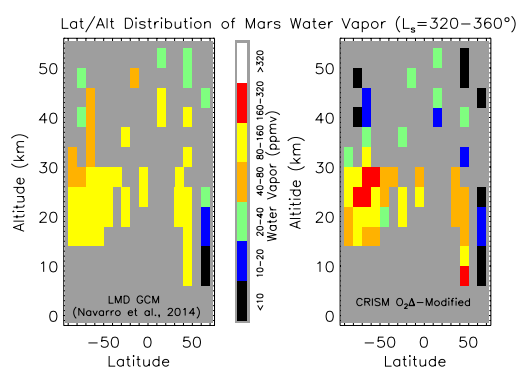


Figure 8. LMDGCM simulated (Navarro et al., 2014) and CRISM $O_2(\Delta_g)$ -scaled water vapor latitude/longitude distributions, averaged over southern spring ($L_s=320-360^\circ$).

Conclusions:

Several general behaviors are indicated in the CRISM-modified water vapor distributions of figures 5-8, including: 1) two-to-three times increased

water vapor above 35-40 km altitudes in all latitudes and seasons, which may indicate reduced supersaturation conditions; 2) stronger confinement of water vapor to northern mid-to-high latitudes in northern spring/summer, which may indicate more effective confinement of water vapor released by the northern ice cap in association with aphelion cloud belt microphysics; and 3) two-to-five times less water vapor at 10-30 km above the southern summer mid-to-high latitudes, which may indicate less effective vertical/meridional transport of water vapor evolved from southern summer polar ice reservoirs.

Bibliography:

- Barth, Hord, Stewart, Lane, Dick, and Andersen, Mariner 9 ultraviolet spectrometer experiment: Seasonal variation of ozone on Mars, *Science*, 795-796 (1973).
- Clancy, Sandor, Wolff, Smith, Lefèvre, Madeleine, Forget, Murchie, F. Seelos, K. Sellos, Nair, Toigo, Humm, Kass, Kleinböhl, and Heavens, Extensive MRO CRISM observations of 1.27 mm O_2 airglow in Mars polar night and their comparison to MRO MCS temperature profiles and LMD GCM simulations, *J. Geophys. Res.*, 117 (2012).
- Clancy, Sandor, García-Muñoz, Lefèvre, Smith, Wolff, Montemessin, Murchie, and Nair, First detection of Mars atmospheric hydroxyl: CRISM near-IR measurement versus LMD GCM simulation of OH Meinel band emission in the Mars polar winter, *Icarus*, 226, 272-281 (2013).
- Clancy, Smith, Lefèvre, McConnochie, Sandor, Wolff, Murchie, Toigo, Nair, and Navarro, Vertical Profiles of Mars 1.27 μm O_2 Dayglow from MRO CRISM Limb Spectra: Seasonal/Global Behaviors, Comparisons to LMDGCM Simulations, and Inferences on Mars Water Vapor Distributions, *Icarus*, in review (2016).
- Guslyakova, Fedorova, Lefèvre, Korablev, Montmessin, Trokhimovsky, and Bertaux, Long-term nadir observations of the O_2 dayglow by SPICAM IR, *Plan. Space. Sci.*, 122, 1-12 (2016).
- Lefèvre, Lebonnois, vMontmessin, and Forget, Three-dimensional modeling of ozone on Mars, *J. Geophys. Res.*, 109 (2004).
- Lefèvre, Bertaux, Clancy, Encrenaz, Fast, Forget, Lebonnois, Montmessin, and Perrier, Heterogeneous chemistry in the atmosphere of Mars, *Nature*, 454, 971-975 (2008).
- McElroy and Donahue, Stability of the Martian atmosphere, *Science*, 177, 986-988 (1972).
- Navarro, Madeleine, Forget, Spiga, Millour, Montmessin, and Määttänen, Global climate modeling of the Martian water cycle with improved microphysics and radiatively active water ice clouds, *J. Geophys. Res.*, 119, 1479-1495 (2014).
- Parkinson and Hunten, Spectroscopy and aeronomy of O_2 on Mars, *J. Atmos. Sci.*, 29, 1380-1390 (1972).